Design and Multi-objective Optimization of a Composite Impact Attenuator for a Formula Student Car

Jose Maria Pinto Basto Cyrne de Castro
josecyrnedecastro@tecnico.ulisboa.pt

Instituto Superior Técnico, Universidade de Lisboa, Portugal

November 2018

Abstract

The need of building lighter, more fuel-efficient aircraft led to an increasing use of composite materials in the aerospace industry over the last few decades. The integration of these materials in energy absorbing structures enticed the study of their crashworthiness and numerical implementation in Finite Element software, in order to correctly predict the complex failure behaviour of composite designs. The current impact attenuator used by the Formula Student team of University of Lisbon is an out-of-shelf solution consisting in an aluminium honeycomb. The competition regulations defined for the impact attenuator's design allow room for innovation, which can be used to build more efficient structures and explore new materials. The main objective of this work is to design and optimize a composite impact attenuator lighter than the solution currently used by University of Lisbon team. Experimental results and numerical model presented in previous work performed by Santos [1] are considered in the development of a new approach. Several design parameters are studied and their influence on the behaviour of the impact attenuators are taken into account. Direct Multisearch (DMS) algorithm directly coupled to Abaqus software is used to perform the optimizations, while different techniques to obtain the best results are introduced. The lighter solutions' mass is compared to the baseline aluminium structure's and detailed descriptions are presented for chosen optimal designs. Final considerations are introduced and further optimization is performed to enhance the results and obtain the final solutions, which constitute an improvement regarding the baseline's mass.
Keywords: Composites, Crashworthiness, Finite Element, Optimization, Formula Student

1. Introduction

The development of composite materials with greater strength-to-weight ratio than metals is one of the cornerstones of the recent innovations in aerospace and automotive industries. The implementation of these materials can lead to significantly lighter structures, ultimately resulting in more fuel efficient and even safer vehicles. However, their complex brittle fracture mechanism makes it difficult to correctly predict their behaviour when subjected to high impact forces, using Finite Element numerical models, which is essential to the innovate design without extensive experimental testing and consequent waste of resources. The Formula Student competition challenges student to design, build and test a racing car while complying with certain regulations. Energy absorption devices are required for safety purposes and their requirements give room for design innovation. Since the team of University of Lisbon currently uses an aluminium honeycomb as the impact attenuator for its car, the opportunity to study the crashworthiness of composite structures emerges. The main goal of this work is to design a composite impact attenuator lighter than the currently used aluminium honeycomb solution. Furthermore, it is intended to assess the influence of different design parameters on the energy absorption capability of the studied impact attenuators and to explore combinations of those factors so that an optimal solution is achieved. This study is a continuation, through a different approach, of the investigation carried out by Santos [1], which numerical model and experimentally obtained material properties are adopted here. The unsuccessful experimental results obtained by Santos [1] were analysed and an alternative optimization is suggested and performed in order to achieve feasible designs.

2. Background

2.1. Composites crashworthiness

As the aerospace and automotive industries transition to an increasing use of composite materials in structures where only metals used to be applied, motivated by stricter emissions guidelines and to attain lighter vehicles with higher fuel efficiency,

the issue of crashworthiness assumes a preponderant role. It is important to ensure that, in replacing metals by composite materials in aircraft and automotive structures, the capability to absorb energy and maintain post-crash integrity is not compromised.

The fracture and failure mechanisms of composite structures during crushing processes are complex, involving micromechanical interactions of the fibre and matrix constituents and their bonded interfaces, failing in a mixture of different modes, namely: (i) matrix cracking fibre tensile breakage, (ii) fibre compressive kinking, (iii) fibre-matrix debonding and (iv) delamination between plies [2–5]. Compared to the buckling and folding deformations common in steel and aluminium under similar loading, the CFRP structures pulverize into small fragments and other fine debris over the duration of the impact load.

Feraboli *et al.* [6] tested the crushing behaviour of different geometries of carbon fibre/epoxy tubes, concluding that curved elements presented greater specific energy absorption (SEA) values comparing to tubes made of flat surfaces only. Hussein *et al.* [7] studied the influence of velocity in hollow and honeycomb-filled composite tubes, obtaining larger values of SEA for the hollow tubes, despite the lower energy absorption attained, and concluded that mean crushing force and SEA, in general, decrease with an increase in impact velocity. Israr *et al.* [8] experimentally obtained the mean crushing stress for an elementary ply, defined as a material characteristic rather, independent of design. The values achieved for 0° plies and 90° plies were similar, meaning both orientations would provide approximately equal energy absorption for a steady impact. However, 0° plies show the possibility for a part of the ply to create steady fragmentation whereas 90° tests turns to global rupture of the ply, which lead to a lower volume of material being involved in the energy absorption process.

Results from composites crashworthiness experimental studies have been used as benchmark for calibration of Finite Element numerical models, using different software, that can predict the complex fracture mechanisms and behaviour of composite structures during failure, but this still poses a challenge since reliability of those models is far lower than the one achieved for the metallic counterparts.

Ramos and Melo [9] compared results of quasi-static crushing of several tubes using two-dimensional and three-dimensional simulations in Abaqus [10] Explicit, Abaqus [10] with CZone [11] application and HyperWorks, both regarding their accuracy compared to experimental tests and the computational cost associated to each software. The influence of parameters such as mesh size, friction coefficient, material properties, impacting mass, tube length and crush stress was studied for each platform. Results obtained using Abaqus [10] with CZone [11] presented the lowest mesh dependency and computational cost associated, but higher structure stiffness was noted, which accounted for the larger accelerations obtained in the simulations. Crush stress parameter was the defined material property which influenced results significantly, when using Abaqus [10] with CZone [11].

To include the effects of delamination in a model must be decided by the user, as there are intrinsic numerical difficulties associated with that phenomenon, which occurs when the bonds between layers of laminate fail due to debonding in the plane of the interface adhesion, reducing the strength, stiffness and load-bearing capacity of the laminate, and consequently influencing the crashworthiness of the structure. Palanivelu *et al.* [12] performed a numerical study on the energy absorption of simple composite tubes with different cross section geometries. Using Abaqus [10] Explicit, delamination effects were included by modelling the tubes with multiple layer of solid cohesive elements between shell layers. This approach produced results that agreed with the experimental ones and the importance of considering delamination in Finite Element models was emphasized.

2.2. Impact attenuators

Going further than the study of simple tubular structures, the crashworthiness of complex composite energy absorbers was already investigated. In the aerospace context, Mou *et al.* [13] studied the influence of composite skin on composite fuselage section crashworthiness through Finite Element analysis performed using LS-DYNA software. Different layups were explored, similarly to what will be done in this investigation. Considering automotive applications, Lescheticky *et al.* [14] successfully predicted the performance of a large car front end made entirely from composites. In this study, as presented by Feraboli *et al.* [6], curved sections attained higher values of SEA, presumed to be caused by suppression of ply delamination ahead of the moving crush front. Moreover, triggers such as a crenelated front end and holes were explored. Regarding the Formula Student competition, Obradovic et al [15] designed an impact attenuator as a truncated pyramid with rounded edges containing a progressive reduction of the wall thickness from the built-in end until the front cross section, which acts as a trigger. Numerical simulations using shell elements (disregarding delamination effects) and experimental tests reached a good level of agreement and several features of this approach were adopted for the present study.

2.3. Multi-objective optimization

Associated to the increase of computational power and software sophistication, optimization has become a valuable tool in the design and improvement of all sorts of components. In problems that require the optimization of multiple objectives, which are often conflictual, a multi-objective optimization is performed, which general formulation is

$$\begin{aligned} \min \quad & F(x) \equiv (f_1(x), f_2(x), ..., f_m(x))^T \\ \text{s.t.} \quad & x \in \Omega \subseteq \mathbb{R}^n \end{aligned} \tag{1}$$

where we have m (≥ 2) objective function components $f_i : \mathbb{R}^n \longrightarrow \mathbb{R} \cup \{+\infty\},\ i = 2, ..., m$, forming the objective function $F(x)$, and Ω represents the feasible region, i.e., the set of points that respect the constraints, which can be defined by mathematical expressions or regarded as an oracle. When user preferences are not defined prior to the optimization process, the Pareto front is captured, which contains only nondominated solutions. Pareto dominance is defined as

$$F(x) \prec_F F(y) \Leftrightarrow F(y) - F(x) \in \mathbb{R}^m_+ \setminus \{0\}. \tag{2}$$

and a certain solution x is said to dominate y ($x \prec y$) when $F(x) \prec_F F(y)$. This concept allows several optimal solutions to be obtained and the user to make an informed decision on which is the best. From one solution of the Pareto front to another, it is not possible to improve an objective function without worsening another (trade-off).

Optimization of energy absorbing structures has been performed for several applications. For the Formula Student competition, Boria *et al.* [16] successfully optimized the thickness of each zone of the impact attenuator presented in [15], similarly to the present work. However, a surrogate model approach was taken and a single objective was considered (SEA), differently to the approach taken here.

The Direct Multisearch (DMS) algorithm developed by Custódio *et al.* [17] is a derivative-free method that uses an extreme barrier approach to deal with constraints, adopting the extreme barrier function to MOO by setting

$$F_\Omega(x) = \begin{cases} F(x) & \text{if } x \in \Omega, \\ (+\infty, ..., +\infty)^T & \text{otherwise.} \end{cases} \tag{3}$$

Equation (3) means that, if a point is infeasible, the values of F_Ω are set to $+\infty$. This allows one to deal with black-box type constraints, such as the case of the present work, where only a binary (yes or no) answer is returned to the optimizer.

The DMS algorithm does not aggregate any of the objective functions. It directly extends, from single to multi-objective optimization, a class of directional derivative-free methods, called direct search. For a certain iterate (poll centre), the poll step evaluates the objective function at some neighbour points. The acceptance of new iterates is done using the Pareto dominance concept. A constant update of the list of nondominated points and corresponding step size parameters is made and, at each iteration, polling is executed at a point of the list with its success being determined by changes in that list.

In this study, DMS directly is used to perform all optimizations.

2.4. Current solution and optimization attempt

Regulations are defined for the impact attenuator (IA) used in the Formula Student competition. Specific minimum dimensions are required, the maximum acceleration (after a 3rd order low-pass Butterworth filter with a cut-off frequency of 100 Hz is applied, if necessary) is set to 40 g's, the average acceleration is limited to 20 g's and an energy absorption of at least 7560 J is imposed. The test is performed by having a mass of 300 kg crashing against the impact attenuator at a minimum speed of 7 m/s. As aerodynamic devices are used by the University of Lisbon team forward of the IA, the maximum acceleration constraint is set to 35 g's, to account for their effects.

Santos [1] performed quasi-static compression crush tests in small carbon fibre coupons, in order to obtain the crush stress parameter necessary for the numerical implementation in Abaqus [10] with the CZone [11] add-on of the material used in this work. The crush stress was measured for different angles.

As previous numerical models built for composite tubes following this methodology obtained reasonable results, it is assumed the implemented model predicted the behaviour of impact attenuators with an acceptable amount of accuracy.

Since initial optimizations of the layup of the structural nose resulted in heavy solutions, a honeycomb foam material was introduced to apply a sandwich structure and enable lighter solutions. The optimization of the IA was done using DMS coupled to Abaqus [10] and considered all dimensions of the structure, number of internal cross section divisions, number of layers on each pair of opposed walls, plies orientation and core inclusion as design variables. This means only parallelepiped-shaped geometries were allowed. The lightweight foam core allowed for a mass minimization up to 67%, comparing to the baseline aluminium solution. The optimal solutions' geometry consisted in rectangular crashboxes with no internal divisions, illustrated in figure 1.

Three final designs were considered by Santos [1]: the first is the solution obtained directly from the optimization, represented in figure 1, the second consists in a similar geometry but adopting the

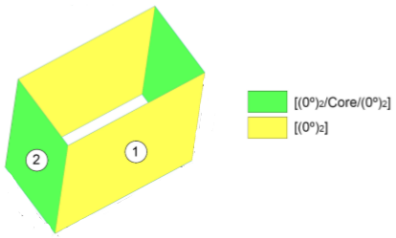

Figure 1: Optimized geometry and layup [1].

sandwich structure in all walls, aiming at a uniform energy absorption in the cross section, and the third is a tube inside a thin box, illustrated in figure 2.

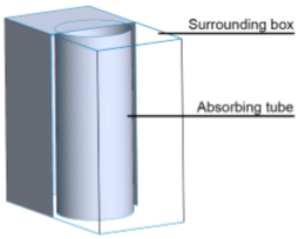

Figure 2: Alternative design [1].

Experimental tests were performed for all three designs and all were considered infeasible, since maximum and average acceleration constraints were violated for the first and second designs, respectively. The third design punctured through the anti-intrusion plate, which is not allowed.

Even though the reasons for the failure of the third design were not well understood by the author (errors associated to the manufacturing process were considered), the first two designs showed that the foam core was completely sheared and delamination between the carbon fibre skins and the core happened, with subsequent loss of transversal stiffness and bending until catastrophic failure.

3. Problem approach

Considering the solutions reviewed and the experimental results obtained by Santos [1] in chapter 2, a different approach to this design and optimization problem was proposed, which main aspects are:

- Honeycomb foam core was not included
- Truncated pyramidal geometries are explored
- Inclusion of a trigger zone through thickness reduction to initiate contact
- Progressive thickening from the trigger until the built-in end will be enforced
- Rounded edges to avoid stress concentration and achieve larger values of SEA
- Definition of zones throughout IA's length to allow more layups variety

4. Multi-objective optimization

4.1. Numerical modelling

The numerical model was constructed in Abaqus [10], with the CZone [11] application incorporated. Initial considerations were made regarding the high computational cost of the finite element analysis and its implication on the overall duration of an optimization process.

Material properties, including the crush stress experimentally obtained in previous work [1], were defined. The impact attenuator was meshed using multi-layered quadrilateral elements with reduced integration, S4R, while the impacting plate was meshed with quadrilateral rigid elements, R3D4. Preliminary studies were made to assess the optimal mesh size and the number of section points per element to be used for the crash simulations performed. Boundary conditions include the encastre of the IA's built-in end, where it is attached to the anti-intrusion plate, and the longitudinal displacement of the rigid barrier. A mass of 300 kg is given to the impacting wall and its velocity is set as a predefined field with a value of 7 m/S. Contact between the impacting barrier and the crashbox is handled by CZone [11] and defined as in the documentation. Self-contact (frictionless, hard) is also included. The Tsai-Wu failure criterion was maintained from previous work. An example of the assembly for a certain model is illustrated in figure 3.

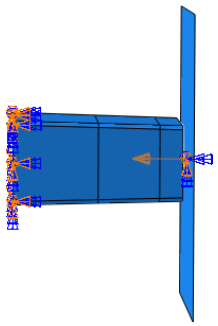

Figure 3: Assembly example.

4.2. Models

All studied models are truncated pyramids with the corners of the cross section rounded with a 5 mm radius. The dimensions of each model are represented in table 1. Smallest and largest cross section (CS) dimensions are defined as width times height.

Firstly, three zones with varying lengths were defined for each model, illustrated in figure 4. Zone A (green) comprises the whole impact attenuator's length, zone B (red) is shorter than zone A and zone C (blue) is shorter than zone B.

The length of each zone for each model is indicated in table 2.

Table 1: Models dimensions

Model	CS dimensions (mm)		Length (mm)
	smallest	largest	
1	200x100	220x110	220
2	220x110	240x120	220
3	220x110	242x121	250

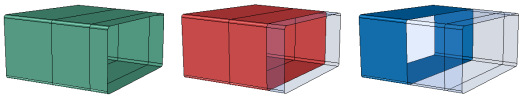

Figure 4: Three zones definition.

Table 2: Length of the three zones

Model	Length (mm)		
	A	B	C
1	220	190	110
2	220	190	110
3	250	220	125

The effect of an extra zone, illustrated in figure 5, is explored in this work.

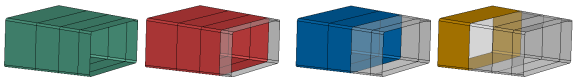

Figure 5: Four zones definition.

The length of each of the four zones defined for each model is indicated in table 3. Two ways of dividing model 1 into four zones (v1 and v2) were explored.

Table 3: Length of the four zones

Model		Length (mm)			
		A	B	C	D
1	**v1**	220	190	140	80
	v2	220	190	110	30
2		220	190	110	30
3		250	190	140	30

Each zone will be assigned with a certain layup. The layup of zone B overlaps the one of zone A over the intersection of their lengths. Similarly, the layup of zone C overlaps the layups of A and B and the layup of zone D, for the four zone models, is applied on top of the others as well.

4.3. Design parameters

Several design parameters were studied throughout the work.

The influence of the tapering of the structure was analysed and it was concluded that higher taper angles lead, generally, to lower accelerations and higher final displacements. However, this feature is implemented to give better stability to the structure in a real case scenario, where the impact is never fully axial. This effect is not included in the numerical simulations, which impact is perfectly axial, therefore, the benefits of this parameter are not visible in the performed analyses, but expected to give better experimental results relative to structures where it is not included. An assessment of the cross section curvature was also performed and results showed that for large values ($\geq$ 25 mm) of radii applied to the rounding of the cross section corners, displacements of the impacting body are much lower (for the same layup), meaning a more effective energy absorption is performed, as highlighted by the literature presented in chapter 2. The influence of the length assigned for each zone in the optimal results obtained was also assessed, using model 1 with four zones. Two different versions, differing only in the zone definition, were submitted to layup optimization and better results were achieved for version 2, which has a short zone D near the built-in end to allow a thick reinforcement of that area without a significant mass penalty.

4.4. Layup optimization

The layup optimization was first defined for geometries containing three zones. Since the crush stress is the most determinant material property in the results of the analyses, three possible ply orientations were allowed: 0° , 30° and 45° , corresponding to the maximum, the minimum and an intermediate value of crush stress, respectively. The multi-objective optimization problem was formulated as follows:

$$\begin{aligned} \min_{x\in\Omega} \quad & F(x) \equiv (m(x), max(A(x)) \\ \text{s.t.} \quad & x_i \in \{0, 30, 45\}, \quad i = 1, \ldots, 4. \\ & x_i \in \{0, 30, 45, 99\}, \quad i = 5, \ldots, 30. \\ & max(A(x)) \leq 35g. \\ & mean(A(x)) \leq 20g. \\ & max(U(x)) < l + g. \end{aligned} \tag{4}$$

Two objective functions are optimized, with particular focus on the minimization of the mass, $m(x)$, while the maximum acceleration, $max(A(x))$, is kept as a performance criterion.

Each design variable, x_i, of the input vector, has the value of the corresponding ply orientation. For every variable containing a value different than 99, a layer is introduced into the corresponding zone layup. Each zone has 10 variables assigned: the first ten, x_1 to x_{10}, concern zone A, while x_{11} to x_{20} correspond to zone B and x_{21} to x_{30} to zone C. Notice how at least four layers are assigned for zone A, since the first four design variables cannot take the value 99.

For optimizations using four zones, an input vector of 28 entries, with seven assigned for each zone,

was introduced, since no optimal solutions having 10 layers were seen in the first results using three zones.

The constraints, which are imposed by Formula Student regulations, are the maximum acceleration, $max(A(x))$, the average acceleration, $mean(A(x))$, and the minimum imposed energy absorption, which is 7350 J. By only considering designs that completely absorb the kinetic energy, fully stopping the impacting barrier, i.e., designs for which the barrier's maximum displacement, $U(x)$), is lower than the sum of the IA's length, l, and the initial gap between both structures, g, we ensure the energy constraint is met, since the 300 kg barrier has an initial velocity of 7 m/s, giving an initial kinetic energy $E_{k_{initial}} = \frac{1}{2}mv^2 = 7350\ J$.

The optimization algorithm used throughout this work is illustrated in figure 6.

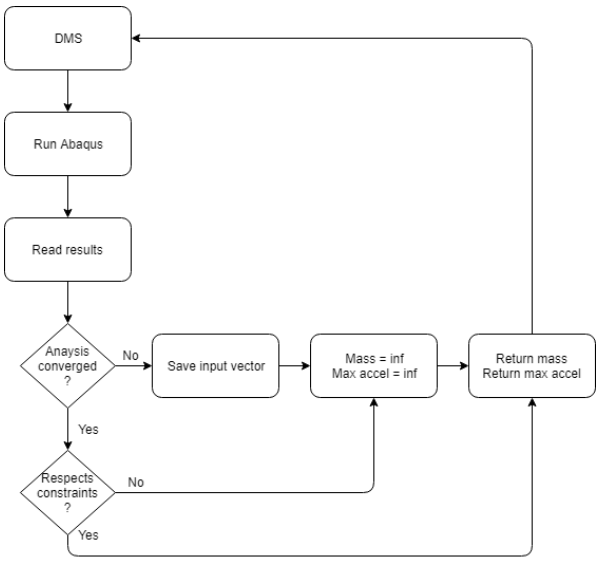

Figure 6: Optimization algorithm.

All optimizations were initialized with a predetermined list of feasible points.

Inputs generated by DMS which have their Finite Element analysis cut short due to convergence issues cannot have their results considered, so they are saved in a text file and their objective functions value is set to "*inf*". A MATLAB [18] program was developed to read those inputs, compare them with the lightest solution obtained from the optimization and re-analyse them in case the their mass is similar to that solution, using a refined barrier mesh, which solved all convergence problems. This process led to the discovery of feasible solutions initially discarded and even a nondominated solution was obtained.

The results obtained using model 1 with three zones are presented in figure 7, with optimal solutions' mass values going from 0.370 kg up to 0.520 kg.

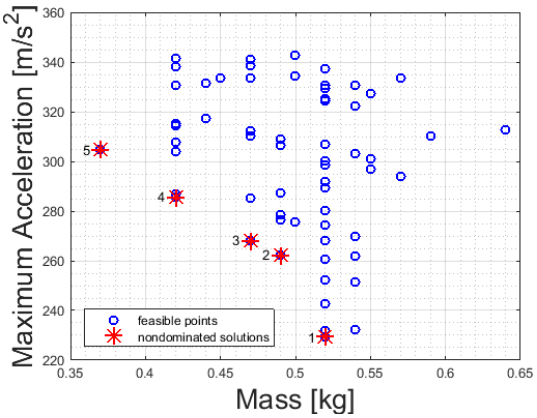

Figure 7: Results for model 1 with three zones.

The addition of an extra zone (zone D) to this model also produced satisfactory results. Two different sets of zones were defined, described as versions 1 and 2 in table 3. Their results are presented in figure 8.

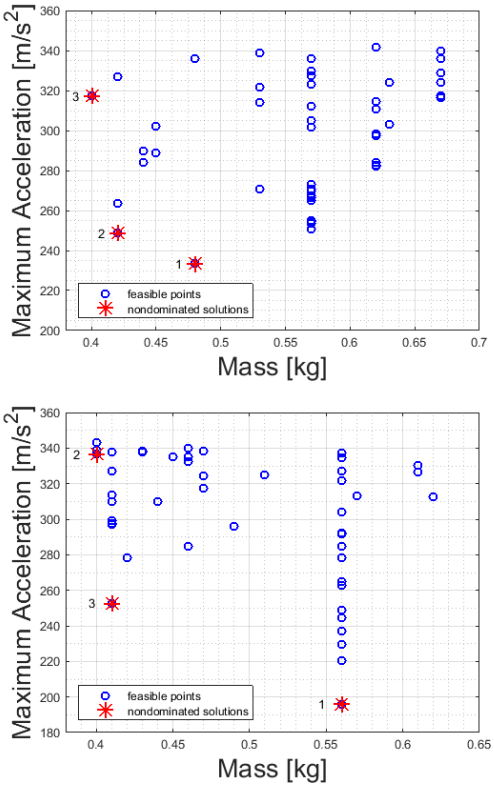

Figure 8: Results for model 1 with four zones. Version 1 results are at the top and version 2 at the bottom.

The lightest solutions obtained for each optimization process constituting the Pareto front represented in figure 8 are described in table 4.

As mass minimization is the main concern and lighter structures were attained for version 2, this

Table 4: Model 1 with four zones - optimal solutions

Version	Solution	Objective function	
		Mass (kg)	Max accel. ($\mathrm{m\,s^{-2}}$)
1	3	0.400	317.15
	2	0.420	248.68
2	2	0.400	336.38
	3	0.410	252.72

zone layout was then implemented for model 2. The addition of a fourth zone in model 2, allowed an improvement of 12% in mass minimization comparing to results obtained using three zones. The results from the optimization process using four zones are illustrated in figure 9.

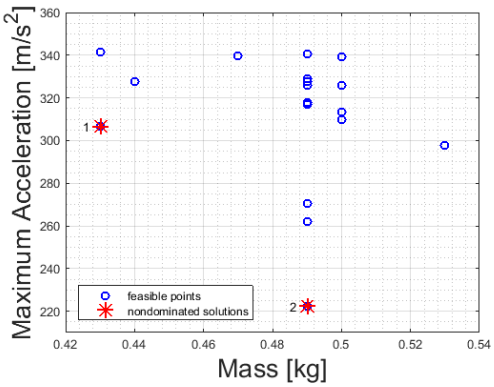

Figure 9: Results for model 2 with four zones.

Optimizations on the layup of model 3 produced only heavy layups, with the lightest having 0.470 kg, due to the large dimensions of the model. A significant improvement also occurs for this model when four zones are used rather than three.

Computational cost of the optimizations depend on the number of function evaluations needed to converge, but elapsed times of up to 4 days were obtained.

The models and layups corresponding to the lightest solutions obtained through optimization are presented in table 5, where the mass reduction (MR) of each solution comparing to the 0.430 kg aluminium impact attenuator is presented.

Table 5: Lightest solutions

Model	Layup				MR
	A	B	C	D	
1	[0,30,30,30]	[45,0]	[30,30]	–	14%
1-v1	[0,30,0,30]	[0]	[0,0,0]	[30]	7%
1-v2	[0,30,0,30]	[0,30]	[0,30]	[0,30,0,30]	7%
1-v2	[0,30,0,30,0]	[30]	[30,30]	[0,30,0,30]	5%
1	[0,30,30,30]	[0,30]	[30,30]	–	2%
2	[0,30,0,30]	[0,30]	[0,30,0,30]	[0,30,30]	0%

The baseline solution was successfully improved, with mass reductions going from 5% up to 14%.

As expected, the exclusive use of carbon fibre and epoxy composite leads to lower mass improvements comparing to the previous work [1], where a honeycomb foam core was allowed in the design, ultimately leading to a mass minimization of 63%. However, the risk of delamination between carbon fibre skins and foam core, observed in the experimental tests performed in [1], is eliminated. Ply orientations of 0° and 30° were the most common and alternated frequently for a certain layup. These orientations seem to complement each other well, since the 0° plies manage to achieve a higher energy absorption due to their higher crush stress, while the 30° plies cause less resistance forces and allow a progressive crushing of the impact attenuator without the occurrence of catastrophic failure.

Dimensions of the model are found to significantly influence results. The first five lightest solutions are achieved by model 1, which has the smallest cross section, while the lightest solution achieved with model 2 managed to match the baseline solution, but not improve it, regarding its mass.

5. Solutions description and improvement

Three impact attenuators were analysed to assess their suitability as the final design.

The solution described in the first row of table 5 and identified as solution 5 in figure 7 was considered, since it represents a significant 14% improvement regarding the baseline's mass. The acceleration curved obtained for this design - impact attenuator 1 -, when subjected to a crash simulation, is represented in figure 10.

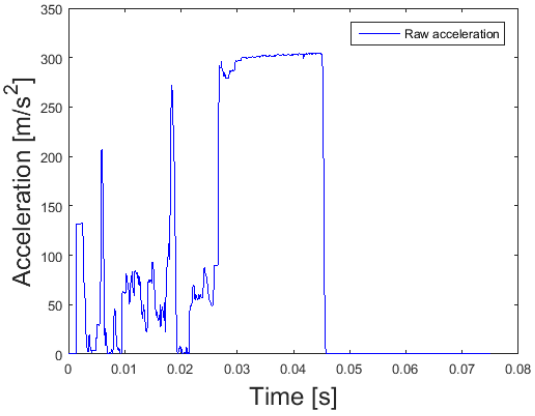

Figure 10: Acceleration over time for IA 1.

Even though it represents a significant improvement regarding the baseline's mass, it presents a maximum acceleration value of 304.76 $\mathrm{m\,s^{-2}}$ (31 g's) and an average acceleration of 16 g's, being both too close to the constraints.

As crash numerical simulations frequently present a significant error, the thin margins associated to

the impact attenuator 1 make it a risky design. Looking at table 4, solution 3 of the version 2 of model 1, using four zones, presents a less significant mass improvement of 5% but a maximum acceleration of 26 g's and average acceleration of 11 g's, which constitute reasonable margins to constraints. The crash simulation was observed and it is illustrated in figure 11.

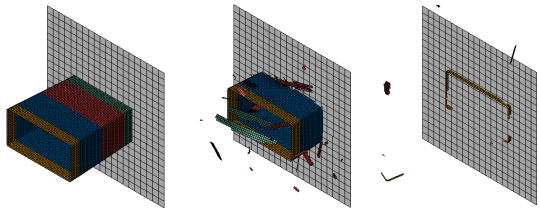

Figure 11: Impact sequence for IA 2.

It is clear, from figure 11, that the length after impact is small (10 mm) and the remaining structure not being entirely intact is a risk, since it means that is has no more energy absorption capacity. This is normal since it is expected that results coming out directly from an optimization are on the limits of the constraints to achieve the best value of the objective functions, when they are conflictual. For this reason, impact attenuator 2 is also considered a risky solution.

Finally, solution described in the last row of table 5 was adopted. Even though it does not constitute an improvement regarding the baseline, it is the only solution on that table that was achieved for model 2. This model cross section dimensions were purposely chosen so that a large range of radii could be applied to the rounding of its corners while complying with the rules, implementing a new design parameter that was explored in section 4.3. Several radii were then applied, while maintaining the layup, and the results were compared in figure 12, where the limit is the distance for which the displacement constraint is violated.

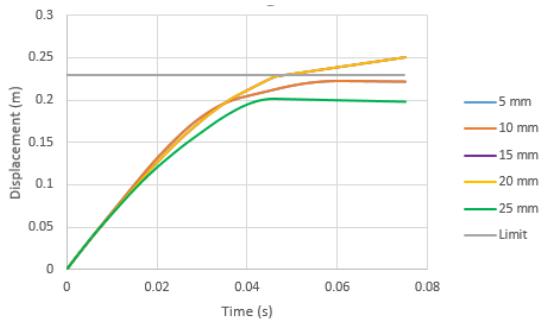

Figure 12: Displacement over time for several radii.

While for a 10 mm radius no significant changes were noticed (curve overlaps the 5 mm curve), for 15 mm and 20 mm the design became infeasible. However, for a 25 mm radius, the structure was more efficient in absorbing the impact energy and the displacement constraint was met by a larger margin. Moreover, the mass is reduced from 0.430 to 0.410, as the perimeter diminishes, which already constitutes an improvement regarding the baseline.

The curves of acceleration over time for the both the original geometry (r=5 mm) and the new one (r=25 mm) were obtained, illustrated in figure 13.

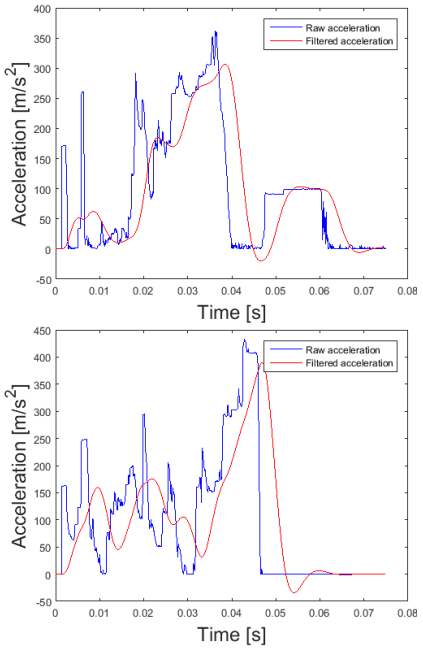

Figure 13: Acceleration curves for different corner radii - r=5mm (top) and r=25mm (bottom).

The acceleration curve of the new geometry, shown in figure 13 (bottom image) present a filtered acceleration peak of approximately 40 g's, which violates the corresponding constraint. Therefore, to turn this design into a feasible one, a multi-objective optimization if performed, formulated as:

$$\begin{aligned} \min_{x\in\Omega} \quad & F(x) \equiv (m(x), max(A(x)) \\ \text{s.t.} \quad & x_i \in \{0, 30\}, \quad i = 1, \ldots, 4. \\ & x_i \in \{0, 30, 99\}, \quad i = 5, \ldots, 14. \\ & max(A(x)) \leq 50g. \\ & mean(A(x)) \leq 20g. \\ & max(U(x)) < l + g. \end{aligned} \tag{5}$$

Similarly to chapter 4, design variables x_i represent a ply orientation, or the absence of one if the value 99 is taken. Only 0° and 30° orientations were allowed, since at this point it is evident they constitute the vast majority of optimal solutions for this problem. Only 14 design variables are used, with 5 assigned for zone A, and 3 assigned for each of the

remaining zones, B, C and D, avoiding the unnecessary evaluation of heavy layups. The minimum number of layers for zone A is 4, since value 99 was not allowed for the first 4 design variables.

Minimizing the maximum acceleration is now not just a performance criterion, but rather a requirement for this design to be considered feasible. In order to accomplish that, the DMS was initialized in the point pretended to be optimized and the maximum acceleration constraint is set to 50 g's so that the DMS does not discard that point, which violated the original limit. Potential further mass minimization will be explored through the multi-objective approach. The remaining original constraints are kept as they are not violated by this solution. Results of this optimization, which performed 77 function evaluations (all numerical simulations converged), are shown in figure 14:

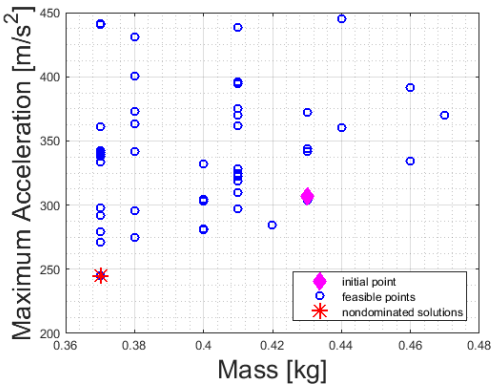

Figure 14: Optimization of new design.

The results show a single optimal solution was achieved, with a mass of 0.370 kg and maximum acceleration of 245.22 $\mathrm{m\,s^{-2}}$, which respects the original constraint of 35 g's. A crash analysis was also performed for this design, so that acceleration and displacement over time could be evaluated.

Through this method, not only is the lightest solution obtained up until this point (impact attenuator 1) matched by this one regarding its mass, but the acceleration peak was also significantly reduced.

For this new solution, margins for the maximum and average accelerations constraints are 29% and 50%. Furthermore, the final displacement of the rigid barrier is reduced, meaning an increase of after-impact length is attained (41 mm, corresponding to an 18% margin regarding the displacement constraint)

Finally, a multi-objective optimization considering both the geometry and the layup of the impact attenuator as design variables was conducted. Four zones were admitted to all generated geometries. The first and second design variables correspond to the length of the crashbox and the length of zone C, respectively, and take possible discrete values assigned for these parameters. The formulation is:

$$
\begin{aligned}
\min_{x\in\Omega} \quad & F(x) \equiv (m(x), max(A(x)) \\
\text{s.t.} \quad & x_i \in \{200, 205, 210, 215, 220\}, \quad i = 1. \\
& x_i \in \{50, 70, 90, 110, 130, 150\}, \quad i = 2. \\
& x_i \in \{0, 30\}, \quad i = 3, \ldots, 6. \\
& x_i \in \{0, 30, 99\}, \quad i = 7, \ldots, 22. \\
& max(A(x)) \leq 35g. \\
& mean(A(x)) \leq 20g. \\
& max(U(x)) < x_1 + g.
\end{aligned}
\tag{6}
$$

The process was initialized in the final solution obtained in chapter 5 (figure 14) and the results are illustrated in figure 15:

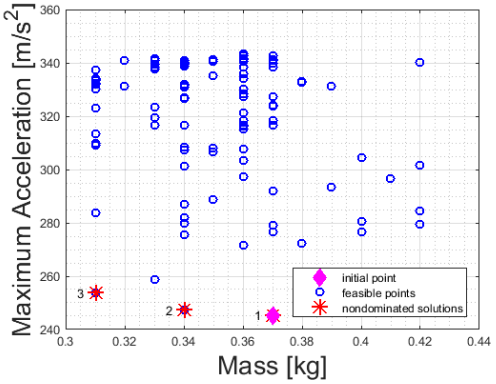

Figure 15: General optimization results.

Results show a Pareto front constituted by the initial point and two others representing a significant mass reduction, with little cost regarding maximum acceleration. Optimal solutions are further described in table 6, where lengths of crashbox (L) and zone C (C) are in milimeters and mass reduction (MR) is a comparison to the aluminium baseline.

Table 6: General optimization - solutions

Solution	L	C	Layup				MR
			A	B	C	D	
1	220	110	[30,30,30,30]	[0,30]	[30]	[30,30]	14%
2	200	110	[30,30,30,30]	[0,30]	[30]	[30,0]	21%
3	200	130	[30,30,30,30]	[0,30]	-	[30]	28%

Mass reduction comparing to the baseline was increased from 14% up to 28%. Maximum accelerations of solutions 2 and 3 are 25 g's and 26 g's, and post-impact lengths are 39 mm and 6 mm, respectively.

6. Conclusions

The present work carries out the design and optimization process of a composite impact attenua-

tor. An assessment of different design parameters is carried out and explored in order to obtain a final lighter structure than the aluminium energy absorber currently used by the FST team of University of Lisbon.

The importance of the crush stress parameter was evident throughout the work, since nearly all optimal solutions presented integrate $0°$ plies or $30°$ plies, which are the corresponding orientations for the maximum and the minimum value of the crush stress, respectively.

Through layup exploration and multi-objective optimization, a feasible design was achieved, which attained a mass reduction of 14% regarding the baseline solution and presented safe margins for all imposed constraints (maximum and average accelerations and final displacement). Finally, considering not only layup but also geometric design variables, mass reduction was improved from 14% up to 28% by performing another successful optimization.

References

[1] André Santos. Dynamic analysis and design of impact attenuator structures for a Formula Student prototype. Master's thesis, Instituto Superior Técnico, June 2017.

[2] B.W.Rosen. Influence of fiber and matrix characteristics on mechanics of deformation and fracture of fibrous composite. *American Society for Metals: Metals Park*, pages 37–75, 1965.

[3] B. Budiansky, N.A. Fleck, and J.C. Amazigo. On kink-band propagation in fiber composites. *Journal of the Mechanics and Physics of Solids*, 46(9):1637 – 1653, 1998.

[4] S.H. Lee and Anthony M. Waas. Compressive response and failure of fiber reinforced unidirectional composites. *International Journal of Fracture*, 100(3):275–306, Dec 1999.

[5] S.H Lee, Chandra S Yerramalli, and Anthony M Waas. Compressive splitting response of glass-fiber reinforced unidirectional composites. *Composites Science and Technology*, 60(16):2957 – 2966, 2000.

[6] Paolo Feraboli, Bonnie Wade, Francesco Deleo, and Mostafa Rassaian. Crush energy absorption of composite channel section specimens. *Composites Part A: Applied Science and Manufacturing*, 40(8):1248 – 1256, 2009. Special Issue: 15th French National Conference on Composites - JNC15.

[7] Rafea Dakhil Hussein, Dong Ruan, Guoxing Lu, and Igor Sbarski. Axial crushing behaviour of honeycomb-filled square carbon fibre reinforced plastic (CFRP) tubes. *Composite Structures*, 140:166 – 179, 2016.

[8] H.A. Israr, S. Rivallant, and J.J. Barrau. Experimental investigation on mean crushing stress characterization of carbonepoxy plies under compressive crushing mode. *Composite Structures*, 96:357 – 364, 2013.

[9] D. Ramos and B. D. Melo. Composite structures impact simulation behavior. Master's thesis, Instituto Superior Técnico, 2014.

[10] Abaqus. Dassault Systmes, Vlizy-Villacoublay, France, 2016.

[11] CZone. Engenuity Ltd., West Sussex, UK, 2016.

[12] S.Palanivelu, W. Van Paepegem, J. Degrieck, D. Kakogiannis, J. Van Ackeren, D. Van Hemelrijck, J. Wastiels, K. De Wolf, and J. Vantomme. Numerical energy absorption study of composite tubes for axial impact loadings. 2009.

[13] Haolei Mou, Tianchun Zou, Zhenyu Feng, and Jian Ren. Crashworthiness simulation research of fuselage section with composite skin. *Procedia Engineering*, 80:59 – 65, 2014. 3rd International Symposium on Aircraft Airworthiness (ISAA 2013).

[14] Juergen Lescheticky, Graham Barnes, and Marc Schrank. System level design simulation to predict passive safety performance for CFRP automotive structures. In *SAE Technical Paper*. SAE International, 04 2013.

[15] Jovan Obradovic, Simonetta Boria, and Giovanni Belingardi. Lightweight design and crash analysis of composite frontal impact energy absorbing structures. *Composite Structures*, 2, 2012.

[16] Simonetta Boria, Jovan Obradovic, and Giovanni Belingardi. On design optimization of a composite impact attenuator under dynamic axial crushing. 45:435–440, 01 2017.

[17] A. Custódio, J. Madeira, A. Vaz, and L. Vicente. Direct multisearch for multiobjective optimization. *SIAM Journal on Optimization*, 21(3):1109–1140, 2011.

[18] MATLAB. Mathworks, Natick, Massachusetts, USA, 2017.